Research in Astron. Astrophys. Vol.0 (200x) No.0, 000–000
http://www.raa-journal.org *http://www.iop.org/journals/raa*

***R**esearch in*
***A**stronomy and*
***A**strophysics*

arXiv:1607.05000v1 [astro-ph.HE] 18 Jul 2016

What determines the observational differences of blazars?

Xu-Liang Fan[1,2,3], Jin-Ming Bai[1,2] and Jirong Mao[1,2]

[1] Yunnan Observatories, Chinese Academy of Sciences, Kunming 650011, China; *fxl1987@ynao.ac.cn, baijinming@ynao.ac.cn*
[2] Key Laboratory for the Structure and Evolution of Celestial Objects, Chinese Academy of Sciences, Kunming 650011, China
[3] University of Chinese Academy of Sciences, Beijing 100049, China

Abstract We examine the scenario that the Doppler factor determines the observational differences of blazars in this paper. Significantly negative correlations are found between the observational synchrotron peak frequency and the Doppler factor. After correcting the Doppler boosting, the intrinsic peak frequency further has a tightly linear relation with the Doppler factor. It is more interesting that this relation is consistent with the scenario that the black hole mass governs both the bulk Lorentz factor and the synchrotron peak frequency. In addition, the distinction of the kinetic jet powers between BL Lacs and FSRQs disappears after the boosting factor δ^2 is considered. The negative correlation between the peak frequency and the observational isotropic luminosity, known as the blazar sequence, also disappears after the Doppler boosting is corrected. We also find that the correlation between the Compton dominance and the Doppler factor exists for all types of blazars. Therefore, this correlation is unsuitable to examine the external Compton emission dominance.

Key words: galaxies: jets — BL Lacertae objects: general — quasars: general — radiation mechanisms: non-thermal

1 INTRODUCTION

Blazar is the most extreme subclass of active galactic nuclei (AGNs). Its radiation is dominated by the non-thermal emission of relativistic jet with small viewing angle to our line of sight. The spectral energy distributions (SEDs) of blazars show two peaks (in $\nu - \nu L_\nu$ diagram) which are believed to be produced by synchrotron and inverse Compton (IC) processes, respectively. However, whether the external photons outside jet participate in the IC process is still an open question (e.g., Chen & Bai 2011; Meyer et al. 2012).

Blazars are classified as flat spectrum radio quasars (FSRQs) and BL Lac objects (BL Lacs) by the optical spectra. They can also be classified as low synchrotron peaked blazars (LSPs), intermediate synchrotron peaked blazars (ISPs), and high synchrotron peaked blazars (HSPs) based on the synchrotron peak frequency (Abdo et al., 2010). An alternative classification based on the ratio of broad line luminosity to Eddington luminosity was proposed by Ghisellini et al. (2011). This classification considers the potential selection effect on the equivalent width (EW) measurement of broad lines due to the Doppler boosting effect, and links the observational classification to accretion regimes. On the other side, the blazar sequence based on the bolometric luminosity was put forward to unify the observational differences of blazars (Fossati et al., 1998). The negative correlations between the peak frequency and luminosity, as well as the Compton dominance (CD) are explained as the increasing cooling from external photons outside jet with increasing luminosity (Ghisellini et al., 1998). However, latter studies

showed that the blazar sequence was an artefact of the Doppler boosting (Nieppola et al., 2008) or redshift selection effects (Giommi et al., 2012), and the sources with both high luminosity and high peak frequency which break the blazar sequence exist (e.g., Padovani et al. 2012; Ackermann et al. 2015). To improve the simple blazar sequence, Meyer et al. (2011) proposed a concept named "blazar envelope" which considered the jet power and the orientation effect. According to the blazar envelope, blazars are composed by two populations divided by jet power, and an envelope forms due to different orientation for various sources.

Since its launch in 2008, the large area telescope (LAT) onboard Fermi gamma-ray space telescope (Fermi) had detected 1444 AGNs in the third LAT catalog (3LAC) clean sample (Ackermann et al., 2015). The broad energy range and high accuracy of LAT promote deep understandings on both the radiation mechanism (e.g. Chen & Bai 2011; Meyer et al. 2012) and the classification of blazars (e.g. Ghisellini et al. 2009; Ghisellini et al. 2011). However, it is still uncertain that the differences of blazars are determined by different physical features, or observational effects (such as the orientation). Moreover, it also needs to be verified that there are one or more factors taking effects on the blazar classifications.

The distinctions of the Doppler boosting had been discovered for different subclasses of blazars, such as BL Lacs and FSRQs (Hovatta et al., 2009), or X-ray-selected BL Lacs and radio-selected BL Lacs (Ghisellini et al., 1993). Stronger Doppler boosting was also suggested to explain the γ-ray detected blazars by many papers (e.g. Kovalev et al. 2009; Lister et al. 2009a; Savolainen et al. 2010; Lister et al. 2015). Furthermore, the blazar sequence was found to be an artefact of the Doppler boosting (Nieppola et al., 2008). All these results indicate that the observational differences of blazars could be determined by the Doppler factor. Thus, this work aims to identify this scenario. Our paper is organized as follows. In section 2, we examine the connection between the Doppler factor and the synchrotron peak frequency. Section 3 presents the impact on jet power due to the Doppler factor. The Doppler-corrected blazar sequence is discussed in section 4. In section 5, we recheck the validity of examining the external Compton (EC) dominance with the correlation between CD and Doppler factor. Discussions are presented in section 6. In this paper, we use a ΛCDM cosmology model with h=0.71, Ω_m=0.27, Ω_Λ=0.73 (Komatsu et al., 2009).

2 SYNCHROTRON PEAK FREQUENCY VERSUS DOPPLER FACTOR

The SED classification of blazars is based on the synchrotron peak frequency. The synchrotron peak frequency, $\nu_{S,p} \propto \gamma_b^2 B\delta$, is related to the electron distribution and the magnetic field strength of the emission region (where γ_b is the break energy of the electron spectrum, B is the magnitude field strength, δ is the Doppler factor. See e.g., Tavecchio et al. 1998). In order to constrain the effect on the blazar classification due to the Doppler factor, we firstly examine the correlation between the Doppler factor and the synchrotron peak frequency. Because the Doppler factor is determined by both the bulk Lorentz factor and the viewing angle ($\delta = [\Gamma(1 - \beta cos\theta)]^{-1}$, where β is the bulk velocity in unit of the speed of light, Γ is the bulk Lorentz factor of relativistic jet, θ is the viewing angle), the wide distribution of these two parameters for both high and low peaked sources have an intense impact on the correlation between the peak frequency and the Doppler factor. Many studies had presented that the γ-ray detected sources had smaller viewing angles (e.g. Savolainen et al. 2010). Thus the less aligned sources are generally excluded for a γ-ray selected sample. For a such sample, the Doppler factor is mainly determined by the intrinsic feature of jet physics, i.e. the bulk Lorentz factor. Therefore, throughout this paper, we just deal with the γ-ray selected samples, and the approximation $\delta \sim \Gamma \sim 1/\theta$ is used.

2.1 Parameter Estimations

The 3LAC provides an ideal γ-ray data set to cross-match with the samples of other bands. In the 3LAC, Ackermann et al. (2015) listed the synchrotron peak frequency estimated by the third-degree polynomial fit. Meanwhile, another method based on the empirical relations proposed by Abdo et al. (2010) was often used in the literatures. Ackermann et al. (2015) compared these two methods, and concluded that

the average offset between the peak frequencies estimated by these two methods was less than 0.26 dex. Because we need to estimate the bolometric luminosity and CD in the following sections, we use the empirical relations in Abdo et al. (2010) to estimate the synchrotron peak frequency throughout this paper. The k-correction is applied as $\nu_{S,p} = \nu^{'}_{S,p}(1+z)$. The Doppler-corrected intrinsic peak frequency is calculated with $\nu_{S,int} = \nu_{S,p}/\delta$. Because the estimation of Doppler factor has large uncertainties and strong dependence on the observational epoch and frequency (Lähteenmäki & Valtaoja, 1999), we use two groups of Doppler factors estimated through two independent methods in this paper. The two groups of results can be cross-checked. For the first method, the brightness temperature is obtained by fitting the variability timescale of radio flux (Lähteenmäki & Valtaoja, 1999), then the Doppler factor is calculated as $(T_{var}/T_{eq})^{1/3}$ (hereafter δ_{var}), where $T_{eq} = 5 \times 10^{10} K$ is the equipartition brightness temperature (Readhead, 1994). For the other method, the core brightness temperature is obtained by fitting the minimum observable size (Readhead, 1994), then $\delta = T_{core}/T_{eq}$ (hereafter δ_{eq}).

Considering the possible variability of the Doppler factors, we search the archive for the Doppler factor during the Fermi era. δ_{var} is derived from Hovatta et al. (2009). Hovatta et al. (2009) estimated δ_{var} for 89 objects (two objects were added from Savolainen et al. 2010). 62 of them have redshift measurement and estimation of $\nu_{S,p}$ in the 3LAC clean sample. There are 39 FSRQs, 16 LSP-BL Lacs (LBLs), 4 ISP BL Lacs (IBLs), 1 HSP-BL Lacs (HBLs) and 2 AGNs of other types in this cross-matching sample. Linford et al. (2012) had observed 232 AGNs with VLBA at 5GHz from 2009 to 2010, and obtained their core brightness temperature. We estimate δ_{eq} with the method described above. $\nu_{S,p}$ is obtained for 139 sources of them. Of these 139 sources, there are 85 FSRQs, 19 LBLs, 13 IBLs, 16 HBLs and 6 AGNs of other types. The details of these two samples are listed in Table 1. The two groups of Doppler factors have very different distributions (Figure 1), while δ_{var} are larger than δ_{eq} to some extent. δ_{var} is derived from the long term radio monitoring. The targets for monitoring are biased for brighter and more variable sources (Lister et al., 2009b), which makes HBLs and IBLs rare for that sample. Therefore, the sources with δ_{var} tend to have large Doppler factors. On the other hand, δ_{eq} estimation is only reliable for low redshift sources, and it can underestimate the real Doppler factor (see detail discussions in Section 2.2).

2.2 Results

The scatters of $\nu_{S,p}$ versus δ_{var} and $\nu_{S,p}$ versus δ_{eq} are plotted in Figure 1. The synchrotron peak frequency $\nu_{S,p}$ is negatively correlated with Doppler factor for both δ_{var} and δ_{eq}, with the correlation coefficient of Spearman rank correlation test $\rho = -0.48$ and the chance probability $P = 8.7 \times 10^{-5}$ for δ_{var}, and $\rho = -0.30$ and $P = 3.4 \times 10^{-4}$ for δ_{eq}. In the right panel of Figure 1, there is no clear trend for each type of sources. The global correlation can be a result of different locations of HBLs and other types of sources (see follows for a possible explanation). As a result of Doppler boosting, we have $\nu_{S,p} = \delta\nu_{S,int}$. Thus the observational peak frequency is expected to be positively correlative with Doppler factor. The opposite trends shown in Figure 1 imply some physical connections between the peak frequency and the Doppler factor.

In order to identify the physical connections, we apply the linear regression to fit the Doppler-corrected peak frequency and the Doppler factor. The input uncertainties are set to 0.3 dex for both sides (Ackermann et al. 2015; Hovatta et al. 2009). The fitting results are

$$log\nu_{S,int} = (-2.54 \pm 0.54) log\delta_{var} + (15.32 \pm 0.56) \quad (1)$$

with the intrinsic scatter 0.14 dex, and

$$log\nu_{S,int} = (-1.83 \pm 0.14) log\delta_{eq} + (14.09 \pm 0.07) \quad (2)$$

with the intrinsic scatter 0.44 dex. The two linear relations are generally consistent with each other, while the latter has a sightly flatter slope (Figure 2). Lähteenmäki & Valtaoja (1999) proposed that during the quiescent state of total flux density, the intrinsic brightness temperature was smaller than the equipartition value. δ_{eq} is estimated through single VLBI observation, thus it underestimates the

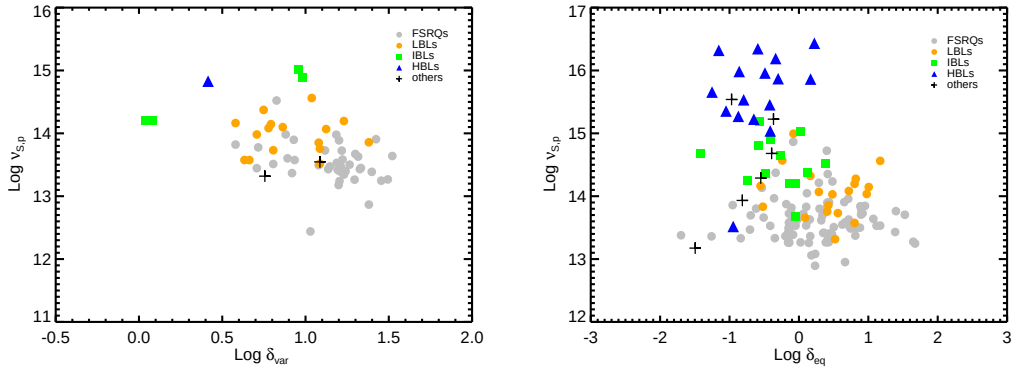

Fig. 1 The correlations between the observational synchrotron peak frequency and the Doppler factor. Different classifications are represented by different symbols as labelled. Left panel: δ_{var} versus $\nu_{S,p}$. Right panel: δ_{eq} versus $\nu_{S,p}$.

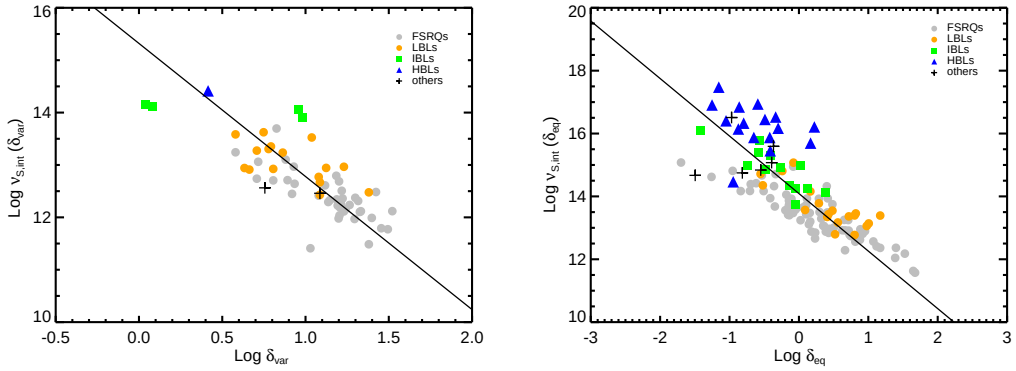

Fig. 2 The correlations between the Doppler-corrected synchrotron peak frequency and the Doppler factor. Different classifications are represented by different symbols as labelled. Left panel: δ_{var} versus $\nu_{S,int}$. Right panel: δ_{eq} versus $\nu_{S,int}$. The solid lines show the best fit.

real Doppler factor for the sources passed the maximum phase of a shock development. This effect may cause the flatter slope between $\nu_{S,int}$ and δ_{eq}. In the right panel of Figure 2, HBLs show different trend with other types of sources clearly. Excluding HBLs, the correlation coefficient between peak frequency and Doppler factor changes to -1.42, which is much flatter than -1.83 in Equation 2. That implies the underestimation to real Doppler factor is more serious for FSRQs and LBLs than for HBLs. One interpretation is that FSRQs and LBLs always locate at higher redshift and are more variable.

3 JET POWER

Meyer et al. (2011) suggested kinetic jet power as an essential feature for the blazar classifications. We thus build a cross-matching sample from the 3LAC clean sample and the sample of Nemmen et al. (2012). This cross-matching sample contains 113 FSRQs and 104 BL Lacs. The distribution of the kinetic jet power for this sample is plotted in Figure 3. The dichotomy between FSRQs and BL Lacs is

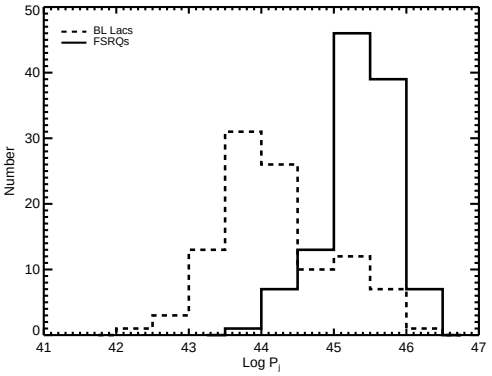

Fig. 3 The distribution of the kinetic jet power. The solid lines correspond to FSRQs, while the dashed lines correspond to BL Lacs.

obvious shown. The Kolmogorov-Smirnov (K-S) test confirms that these two subclasses are draw from distinct samples with D = 0.67 and probability = 1.9×10^{-22}. Because the material energy loading in jets is also boosted by the jet speed with a factor of Γ^2 (e.g. Celotti & Ghisellini 2008), the distribution of the kinetic jet power is also influenced by the Doppler factor. We estimate the material energy in the comoving frame (hereafter intrinsic jet power) with $P_{j,int} = P_j/\Gamma^2 \sim P_j/\delta^2$. The sample with δ_{var} estimation has 33 FSRQs and 20 BL Lacs, while 40 FSRQs and 44 BL Lacs have δ_{eq} estimations. The details of these two samples are also combined in Table 1. The distributions of $P_{j,int}$ calculated by two groups of δ are plotted in Figure 4. BL Lacs and FSRQs roughly have the same range of $P_{j,int}$. The null hypotheses that FSRQs and BL Lacs are draw from the same distribution are not rejected by the K - S tests, with D= 0.34, probability = 0.09 and D= 0.18, probability = 0.49 for the intrinsic jet power calculated by δ_{var} and δ_{eq}, respectively. FSRQs and BL Lacs are suggested to locate in distinct accretion regimes (e.g., Ghisellini et al. 2011). If this is the case, our results indicate that the material energy of jet is independent on the accretion mode. The distinctions of jet power between FSRQs and BL Lacs are mainly caused by the jet speed which is related to the jet acceleration processes or the gas environments in the host galaxies. Therefore, the assumption that the jet power is proportional to the accretion rate (e.g. Ghisellini & Tavecchio 2008) should be used carefully.

4 BLAZAR SEQUENCE

Nieppola et al. (2008) found that the negative correlation between the peak frequency and luminosity became positive after the Doppler boosting was corrected. Thus we examine the Doppler-corrected blazar sequence for our samples. The Doppler-corrected intrinsic bolometric luminosity is calculated as follows. The isotropic luminosity L_{iso} is firstly obtained by combing the synchrotron peak luminosity and IC peak luminosity, where the synchrotron peak luminosity $L_S = \nu_{S,p}L_{S,p} = 4\pi {d_L}^2 \nu^{'}_{S,p} F^{'}_{S,p}$, IC peak luminosity $L_{IC} = \nu_{IC,p}L_{IC,p} = 4\pi {d_L}^2 \nu^{'}_{IC,p} F^{'}_{IC,p}$. The peak flux of synchrotron emission $F^{'}_{S,p}$ and the peak frequency of IC process $\nu^{'}_{IC,p}$ are estimated through the empirical relations from Abdo et al. (2010). The flux of IC peak $F^{'}_{IC,p}$ is estimated by extrapolating the LAT flux to IC peak. Because the radiation of blazar is highly anisotropic, the realistic solid angle of the anisotropic emission is $2\pi(1 - cos\theta_j)$ corresponding to the jet opening angle $2\theta_j$. However, the isotropic luminosity is calculated assuming the solid angle 4π. The deviation is $(1 - \cos\theta_j)/2 \sim \theta_j^2/4 \sim 1/4\delta^2$ for small opening angles. Meanwhile, according to a moving, isotropic jet model, the boosting factor of the luminosity is considered as $\nu L_\nu = \delta^{4+\alpha} \nu^{iso} L_\nu^{iso}$, where L_ν^{iso} is the intrinsic monochromatic luminosity in comoving frame, L_ν is beamed monochromatic luminosity, α is the spectral index, which is taken as 1

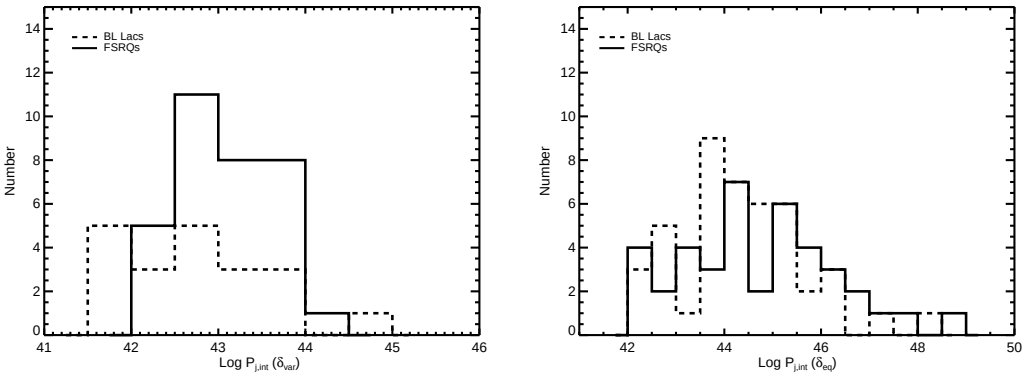

Fig. 4 The distributions of the intrinsic jet power.The solid lines correspond to FSRQs, while the dashed lines correspond to BL Lacs. Left panel is calculated by δ_{var}, while right panel is calculated by δ_{eq}.

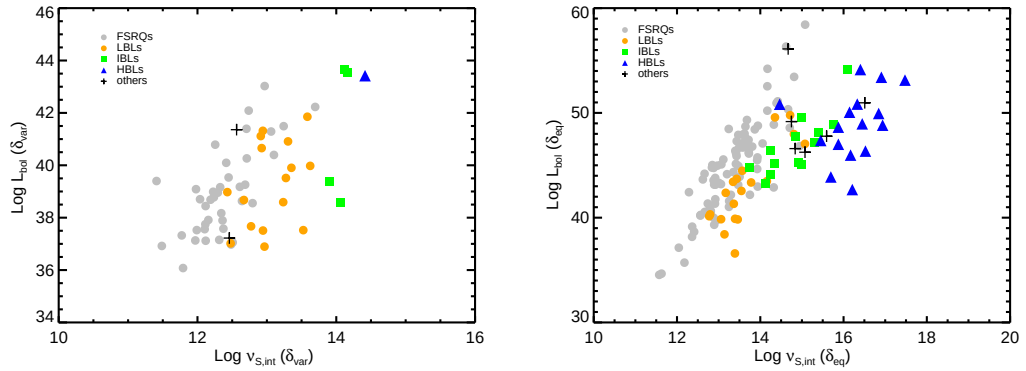

Fig. 5 The correlations between the Doppler-corrected synchrotron peak frequency and bolometric luminosity. Different classifications are represented by different symbols as labelled. Left panel is calculated by δ_{var}, while right panel is calculated by δ_{eq}.

around the peak (Urry & Padovani 1995; Nieppola et al. 2008). Thus the intrinsic bolometric luminosity is estimated as $L_{bol} \sim L_{iso}/4\delta^7$.

There show apparently positive correlations between $\nu_{S,int}$ and L_{bol} in Figure 5. However, after removing the common dependence on the Doppler factor of these two parameters with the partial Kendall's τ correlation test (Akritas & Siebert, 1996), no correlation exists between them. The correlation coefficients τ and the chance probabilities P are 0.01 and 0.87 for the parameters calculated with δ_{var}, and 0.04 and 0.24 for those calculated with δ_{eq}. The anti-correlation between observational peak frequency and luminosity disappears after the Doppler boosting is corrected. Thus the blazar sequence is a result of the Doppler boosting. Ghisellini et al. (1998) explained the anti-correlation between the observational peak frequency and luminosity as the consequence of the anti-correlation between the break energy of electron spectrum and the strength of EC radiation, and proposed that the increasing cooling from the external photons led to both the decrease of the peak frequency and the increase of the luminosity. Our results indicate that the cooling effect seems unimportant to determine the peak

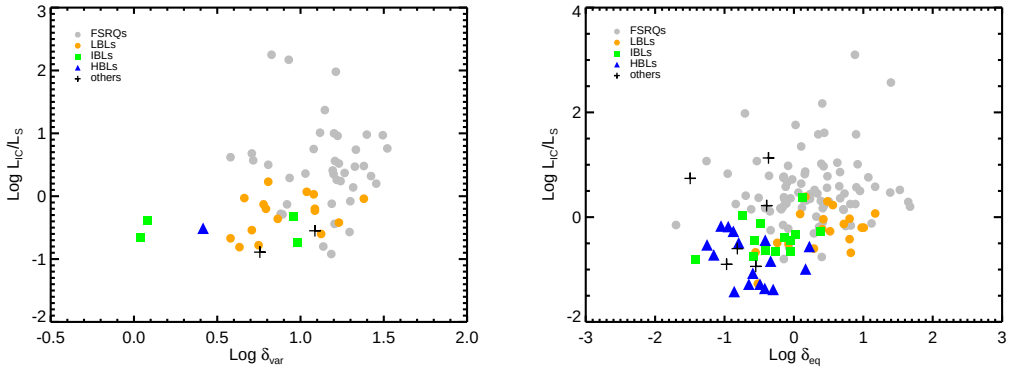

Fig. 6 The correlations between the Compton dominance and the Doppler factor. Different classifications are represented by different symbols as labelled. Left panel: δ_{var} versus CD. Right panel: δ_{eq} versus CD.

frequency because the intrinsic luminosity has no correlation with the peak frequency. Recently, Chen (2014) found a significant correlation between the synchrotron peak frequency and the curvature of the SEDs. Their result also implied that the break energy of electron spectrum γ_b was mainly determined by the particle acceleration process (also see the reference therein). Then the different γ_b result in different peak frequency. On the other hand, the different magnetic fields of the emission region also result in various observational features on peak frequency.

Similar with Figure 1 and Figure 2, HBLs show an additional track on the right panel of Figure 5. This could be caused by different physical features between HBLs and other blazars, such as the radiative efficiency or the radiation mechanism. We examine the correlation between $\nu_{S,int}$ and L_{bol} for the sample excluding HBLs. The result of the partial correlation test still shows no correlation existing between these two parameters, with τ = 0.07 and P = 0.07. For HBLs alone, there is also no correlation between $\nu_{S,int}$ and L_{bol}, with τ = 0.05 and P = 0.7. On the other side, the additional track of HBLs can also be caused by the underestimation of δ_{eq} to the real Doppler factor (Lähteenmäki & Valtaoja 1999, Section 2.2). Because the current sample of δ_{var} has rare HBLs, a completed sample of δ_{var} derived from the radio monitoring programmes, e.g., OVRO (Richards et al., 2011), would help to confirm this trend in the future.

5 EXTERNAL COMPTON EMISSION

Meyer et al. (2012) found a correlation between CD and δ for the very high power sources (including radio galaxies and blazars). They explained that the high energy components of these sources were dominated by EC process rather than synchrotron self-Compton (SSC) process. Then they suggested this correlation to examine the EC dominance for blazars. We plot the scatters of CD and δ in Figure 6 for our samples. There are weak correlations between CD and δ for all sources, with ρ = 0.37, $P = 3.4 \times 10^{-3}$ for δ_{var}, and ρ = 0.32, $P = 1.1 \times 10^{-4}$ for δ_{eq}. More importantly, HBLs have the same trend on the CD-δ plane with LBLs and FSRQs (right panel of Figure 6).

For SSC process, if the ratio of synchrotron energy density to magnetic field energy density $u_{syn}/u_B \simeq CD \propto \gamma_b^3 N(\gamma_b)/R^2$ is independent on Doppler factor (where $N(\gamma_b)$ is the electron number at the break energy γ_b, R is the radius of the emission region. See e.g. Finke 2013), the correlation of CD and δ only exists for EC process. However, if either the electron distribution or the radius of emission region changes with the bulk Lorentz factor (the viewing angle seems impossible to be correlative with these parameters as a coincidence), the correlation between CD and δ is also expected for SSC process. As the result of the adiabatic expansion, the radius of emission region is the cross sectional radius of a

cone. We have $R \sim r\theta_j \sim r/\Gamma$, where r is the distance between the emission region and the central nucleus, θ_j is the opening angle of the jet (e.g., Sikora et al. 2009). Thus the increase of Γ results in the decrease of R. As a result, CD increases as Γ increases. This means that the correlation between CD and δ also exists for the SSC dominant sources. However, if CD correlated with δ is not unique for EC emission, this trend will be unsuitable to examine the EC dominance.

6 DISCUSSIONS

The viewing angles of the γ-ray detected blazars are small, then the bulk Lorentz factors Γ approximately equal to the Doppler factors δ (Savolainen et al., 2010). Thus the trends found for the Doppler factor are mainly determined by the bulk Lorentz factor. Our correlation analyses between the Doppler-corrected peak frequency and bolometric luminosity indicate that the electron acceleration processes or the magnetic field of the emission region determines the peak frequency. The correlation between the peak frequency and the Doppler factor further presents a connection between peak frequency and bulk Lorentz factor. Meanwhile, the distinction of the kinetic jet power is also caused by the bulk Lorentz factor. Therefore, we can expect that the differences of blazars are determined by a single parameter, i.e., the bulk Lorentz factor. Meyer et al. (2011) discussed the possibility of the structured jets with velocity gradients. The radiations of the sources with large viewing angles are dominated by the slow regions. Then varying viewing angles forms an observational sequence. Similarly to that, different bulk Lorentz factors for individual blazars can directly lead to the same observational appearance.

One scenario to explain the different bulk Lorentz factors was suggested by Potter & Cotter (2013b). They explained that the bulk Lorentz factor was governed by the accretion rate, and the black hole masses were similar for all blazars. The higher accretion rate leads to smaller mass loading into the jets, then larger fraction of the accretion power are converted to accelerate the jet. Finally it results in larger bulk Lorentz factor. Our results seems to rule out this scenario because the material energy loading in jets (i.e., the intrinsic jet power) is independent on the accretion rate (see Section 3). Chai et al. (2012) found a significant correlation between the bulk Lorentz factor and black hole mass, but no correlation between the bulk Lorentz factor and the Eddington ratio. Their results also suggest that the bulk Lorentz factor is independent on the accretion rate, but governed by the black hole mass. Potter & Cotter (2013a) also presented another scenario to unify the jet physics. They assumed that the radius of transition region (where the jet comes into equipartition between magnetic filed energy and particle energy, and dominates the optically thin synchrotron emission) scaled linearly with black hole mass. Therefore, the larger black hole mass leads to the farer transition region from the central black hole. This further results in lower magnetic field strength, finally results in lower synchrotron peak frequency. Based on another assumption that the intrinsic jet power has a fixed fraction of the Eddington luminosity (i.e. the intrinsic jet power is independent on accretion rate), they got a relation between the synchrotron peak frequency and the black hole mass with the form $\nu_{S,int} \propto M_{BH}^{-1/2}$. Observationally, The anti-correlation between the peak frequency and black hole mass has been found by e.g., Chen & Bai (2011). When combined this relation with $\Gamma \propto M_{BH}^{0.2}$ found by Chai et al. (2012), we have $\nu_{S,int} \propto \Gamma^{-2.5}$. This relation agrees well with our findings presented in Equations (1) and (2). Therefore, the SEDs of blazars are mainly determined by the black hole mass, but not the luminosity (Ghisellini et al., 1998), accretion rate (Ghisellini et al., 2009), or orientation (Meyer et al., 2011).

7 CONCLUSION

In this paper, we obtain two groups of Doppler factors estimated through two independent methods, aim to identify whether the Doppler factor determines the observational differences of blazars. Significant correlations are found between the Doppler factors and the indicator of the SED classification, i.e., observational synchrotron peak frequency. After corrected the Doppler boosting, the intrinsic peak frequency has uniform linear relations with two groups of Doppler factors. In addition, we find the distinction of jet power is mainly caused by the different Doppler factors for different subclasses. The negative correlation between the peak frequency and the observational isotropic luminosity disappears after the

Doppler boosting is corrected. All these results confirm that the Doppler factor (physically the bulk Lorentz factor) determines the observational differences of blazars. Furthermore, the black hole mass plays an important role to control the bulk Lorentz factor and SED of blazars. Moreover, we find the correlation between the Compton dominance and the Doppler factor existing for all types of blazars, thus this correlation is unsuitable to examine the EC emission dominance. The correlation between CD and Doppler factor can be explained for SSC process if the radius of emission region decreases as the bulk Lorentz factor increases.

Acknowledgements We thank the anonymous referee for his/her useful comments. We are also grateful to Yi-Bo Wang, Liang Chen and Neng-Hui Liao for their useful discussions which improve this manuscript intensively. This research is supported by the Strategic Priority Research Program of the Chinese Academy of Sciences - The Emergence of Cosmological Structures (grant No. XDB09000000), the Key Research Program of the Chinese Academy of Sciences (grant No. KJZD-EW-M06), and the NSFC through NSFC-11133006 and 11361140347. J. Mao is supported by the Hundred-Talent Program of Chinese Academy of Sciences.

References

Abdo, A. A., Ackermann, M., Agudo, I., et al. 2010, ApJ, 716, 30
Acero, F., Ackermann, M., Ajello, M., et al. 2015, ApJS, 218, 23
Ackermann, M., Ajello, M., Atwood, W. B., et al. 2015, ApJ, 810, 14
Akritas, M. G., & Siebert, J. 1996, MNRAS, 278, 919
Celotti, A., & Ghisellini, G. 2008, MNRAS, 385, 283
Chai, B., Cao, X., & Gu, M. 2012, ApJ, 759, 114
Chen, L. 2014, ApJ, 788, 179
Chen, L., & Bai, J. M. 2011, ApJ, 735, 108
Finke, J. D. 2013, ApJ, 763, 134
Fossati, G., Maraschi, L., Celotti, A., Comastri, A., & Ghisellini, G. 1998, MNRAS, 299, 433
Ghisellini, G., Celotti, A., Fossati, G., Maraschi, L., & Comastri, A. 1998, MNRAS, 301, 451
Ghisellini, G., Maraschi, L., & Tavecchio, F. 2009, MNRAS, 396, L105
Ghisellini, G., Padovani, P., Celotti, A., & Maraschi, L. 1993, ApJ, 407, 65
Ghisellini, G., & Tavecchio, F. 2008, MNRAS, 387, 1669
Ghisellini, G., Tavecchio, F., Foschini, L., & Ghirlanda, G. 2011, MNRAS, 414, 2674
Giommi, P., Padovani, P., Polenta, G., et al. 2012, MNRAS, 420, 2899
Hovatta, T., Valtaoja, E., Tornikoski, M., & Lähteenmäki, A. 2009, A&A, 494, 527
Komatsu, E., Dunkley, J., Nolta, M. R., et al. 2009, ApJS, 180, 330
Kovalev, Y. Y., Aller, H. D., Aller, M. F., et al. 2009, ApJ, 696, L17
Lähteenmäki, A., & Valtaoja, E. 1999, ApJ, 521, 493
Linford, J. D., Taylor, G. B., Romani, R. W., et al. 2012, ApJ, 744, 177
Lister, M. L., Aller, M. F., Aller, H. D., et al. 2015, ApJ, 810, L9
Lister, M. L., Homan, D. C., Kadler, M., et al. 2009a, ApJ, 696, L22
Lister, M. L., Cohen, M. H., Homan, D. C., et al. 2009b, AJ, 138, 1874
Meyer, E. T., Fossati, G., Georganopoulos, M., & Lister, M. L. 2011, ApJ, 740, 98
Meyer, E. T., Fossati, G., Georganopoulos, M., & Lister, M. L. 2012, ApJL, 752, L4
Nemmen, R. S., Georganopoulos, M., Guiriec, S., et al. 2012, Science, 338, 1445
Nieppola, E., Valtaoja, E., Tornikoski, M., Hovatta, T., & Kotiranta, M. 2008, A&A, 488, 867
Padovani, P., Giommi, P., & Rau, A. 2012, MNRAS, 422, L48
Potter, W. J., & Cotter, G. 2013a, MNRAS, 431, 1840
Potter, W. J., & Cotter, G. 2013b, MNRAS, 436, 304
Readhead, A. C. S. 1994, ApJ, 426, 51
Richards, J. L., Max-Moerbeck, W., Pavlidou, V., et al. 2011, ApJS, 194, 29
Savolainen, T., Homan, D. C., Hovatta, T., et al. 2010, A&A, 512, A24

Sikora, M., Stawarz, Ł., Moderski, R., Nalewajko, K., & Madejski, G. M. 2009, ApJ, 704, 38
Tavecchio, F., Maraschi, L., & Ghisellini, G. 1998, ApJ, 509, 608
Urry, C. M., & Padovani, P. 1995, PASP, 107, 803

Table 1 Source Data

3FGL name	z	opt.	SED	$\nu_{S,p}$	CD	δ_{var}	$\nu_{S,int}$	L_{bol}	$P_{j,int}$	δ_{eq}	$\nu_{S,int}$	L_{bol}	$P_{j,int}$
J0006.4+3825	0.23	FSRQ	LSP	13.58	0.77	-	-	-	-	-0.14	13.72	46.25	-
J0050.6-0929	0.63	BL Lac	ISP	14.88	-0.74	0.98	13.90	39.38	42.35	-	-	-	-
J0058.3+3315	1.37	FSRQ	LSP	13.51	0.45	-	-	-	-	0.73	12.79	41.10	-
J0108.7+0134	2.10	FSRQ	LSP	13.50	0.37	1.26	12.24	38.78	43.93	-	-	-	-
J0109.1+1816	0.44	BL Lac	HSP	15.96	-1.28	-	-	-	-	-0.49	16.45	48.96	-
J0112.1+2245	0.26	BL Lac	ISP	15.02	-0.33	0.96	14.06	38.57	41.83	0.02	15.00	45.11	43.70
J0112.8+3207	0.60	FSRQ	ISP	14.86	-0.22	-	-	-	-	-0.08	14.95	46.84	45.37
J0113.4+4948	0.39	FSRQ	LSP	13.26	-0.15	-	-	-	-	-0.16	13.42	46.14	-
J0137.0+4752	0.86	FSRQ	LSP	13.63	0.14	1.32	12.31	37.15	42.15	0.72	12.91	41.34	43.34
J0151.6+2205	1.32	FSRQ	LSP	13.45	0.68	0.71	12.74	42.09	-	-	-	-	-
J0204.8+3212	1.47	FSRQ	LSP	13.76	2.57	-	-	-	-	1.40	12.36	39.14	42.53
J0217.5+7349	2.37	FSRQ	LSP	13.90	2.17	0.93	12.97	43.02	43.15	0.41	13.49	46.67	44.19
J0221.1+3556	0.94	FSRQ	LSP	-	-	-	-	-	-	-1.17	-	-	47.91
J0222.6+4301	0.44	BL Lac	HSP	14.83	-0.51	0.41	14.41	43.42	44.60	-	-	-	-
J0237.9+2848	1.21	FSRQ	LSP	13.39	0.56	1.21	12.19	38.69	43.18	0.48	12.92	43.79	44.64
J0238.6+1636	0.94	BL Lac	LSP	13.86	-0.04	1.38	12.48	37.02	41.96	0.42	13.43	43.71	43.87
J0245.4+2410	2.24	FSRQ	LSP	13.36	1.07	-	-	-	-	-1.26	14.62	56.33	-
J0310.8+3814	0.94	FSRQ	LSP	13.96	0.15	-	-	-	-	0.71	13.25	41.03	-
J0325.2+3410	0.06	NLSY1	HSP	15.23	1.13	-	-	-	-	-0.37	15.59	47.77	-
J0325.5+2223	2.07	FSRQ	LSP	13.41	1.61	-	-	-	-	0.44	12.97	44.96	-
J0339.5-0146	0.85	FSRQ	LSP	13.40	0.24	1.24	12.16	37.91	42.83	-	-	-	-
J0423.2-0119	0.92	FSRQ	LSP	13.67	-0.08	1.30	12.37	37.58	42.64	-	-	-	-
J0433.6+2905	0.97	BL Lac	LSP	14.99	-0.51	-	-	-	-	-0.08	15.07	47.05	-
J0449.0+1121	2.15	FSRQ	LSP	13.81	1.02	-	-	-	-	0.39	13.41	45.14	44.43
J0501.2-0157	2.29	FSRQ	LSP	13.18	0.35	1.20	11.98	39.09	43.90	-	-	-	-
J0509.3+1012	0.62	FSRQ	LSP	13.71	0.66	-	-	-	-	-0.10	13.81	46.78	-
J0510.0+1802	0.42	FSRQ	LSP	13.26	0.35	-	-	-	-	-0.14	13.40	46.38	-
J0530.8+1330	2.07	FSRQ	LSP	13.27	0.97	1.49	11.77	37.32	42.93	0.43	12.84	44.79	45.06
J0608.0-0835	0.87	FSRQ	ISP	13.98	-0.28	0.88	13.10	40.40	43.66	-	-	-	-
J0612.8+4122	-	BL Lac	ISP	-	-	-	-	-	-	0.02	-	-	43.70
J0638.6+7324	1.85	FSRQ	LSP	13.62	0.72	-	-	-	-	-0.02	13.65	47.59	-
J0650.7+2503	0.20	BL Lac	HSP	16.32	-0.72	-	-	-	-	-1.15	17.48	53.13	-
J0654.4+4514	0.93	FSRQ	LSP	-	-	-	-	-	-	-0.48	-	-	46.05
J0654.4+5042	1.25	FSRQ	ISP	14.37	-0.25	-	-	-	-	-0.34	14.71	48.58	44.29
J0710.5+4732	1.29	BL Lac	ISP	14.37	0.37	-	-	-	-	0.12	14.25	46.40	45.35
J0712.6+5033	0.50	BL Lac	LSP	13.66	0.06	-	-	-	-	0.09	13.57	44.48	-
J0719.3+3307	0.78	FSRQ	ISP	13.80	0.52	-	-	-	-	0.30	13.50	43.90	-
J0721.9+7120	0.13	BL Lac	LSP	14.56	0.07	1.04	13.52	37.52	42.69	1.17	13.39	36.59	42.42
J0725.2+1425	1.04	FSRQ	ISP	13.60	0.28	-	-	-	-	-0.12	13.72	47.43	-
J0738.1+1741	0.42	BL Lac	LSP	14.16	-0.67	0.58	13.58	41.85	43.31	-0.55	14.72	49.78	45.58
J0739.4+0137	0.19	FSRQ	ISP	13.58	0.29	0.93	12.64	38.64	42.23	-	-	-	-
J0742.6+5444	0.72	FSRQ	ISP	13.85	0.50	-	-	-	-	0.95	12.89	39.32	-
J0746.4+2540	2.98	FSRQ	LSP	13.50	3.10	-	-	-	-	0.88	12.62	43.65	-

Table 1 continued.

3FGL name	z	opt.	SED	$\nu_{S,p}$	CD	δ_{var}	$\nu_{S,int}$	L_{bol}	$P_{j,int}$	δ_{eq}	$\nu_{S,int}$	L_{bol}	$P_{j,int}$
J0750.6+1232	0.89	FSRQ	LSP	13.49	-0.16	-	-	-	-	0.82	12.67	40.55	-
J0757.0+0956	0.27	BL Lac	LSP	14.37	-0.78	0.75	13.62	39.98	42.84	-	-	-	-
J0805.4+6144	3.03	FSRQ	LSP	13.27	1.76	-	-	-	-	0.02	13.24	48.47	-
J0809.6+3456	0.08	BL Lac	HSP	15.45	-1.36	-	-	-	-	-0.42	15.87	47.01	-
J0809.8+5218	0.14	BL Lac	HSP	15.66	-0.53	-	-	-	-	-1.25	16.91	53.40	45.79
J0814.7+6428	0.24	BL Lac	LSP	14.32	0.39	-	-	-	-	0.16	14.16	43.48	-
J0816.7+5739	-	BL Lac	HSP	-	-	-	-	-	-	-2.00	-	-	48.01
J0818.2+4223	0.53	BL Lac	LSP	13.57	-0.03	0.66	12.91	41.11	43.08	0.80	12.77	40.14	42.81
J0824.9+5551	1.42	FSRQ	LSP	13.50	0.58	-	-	-	-	-0.12	13.62	48.01	-
J0830.7+2408	0.94	FSRQ	LSP	13.73	1.01	1.12	12.61	39.18	42.99	0.92	12.81	40.57	43.38
J0834.1+4223	0.25	FSRQ	ISP	13.82	0.26	-	-	-	-	-0.11	13.92	45.48	44.40
J0841.4+7053	2.22	FSRQ	LSP	13.47	1.98	1.21	12.26	40.79	43.55	-0.71	14.17	54.21	47.38
J0850.2-1214	0.57	FSRQ	LSP	13.72	0.26	1.22	12.51	37.06	-	-	-	-	-
J0854.8+2006	0.31	BL Lac	LSP	14.20	-0.42	1.23	12.97	36.89	41.71	0.80	13.39	39.89	42.57
J0915.8+2933	-	BL Lac	HSP	-	-	-	-	-	-	-0.59	-	-	44.93
J0920.9+4442	2.19	FSRQ	LSP	13.72	0.38	-	-	-	-	-0.14	13.87	48.43	46.13
J0921.8+6215	1.45	FSRQ	LSP	13.51	0.30	-	-	-	-	0.50	13.01	43.32	44.66
J0929.4+5013	-	BL Lac	ISP	-	-	-	-	-	-	-0.02	-	-	44.13
J0937.7+5008	0.28	FSRQ	LSP	13.62	0.01	-	-	-	-	0.32	13.29	42.18	-
J0945.9+5756	0.23	BL Lac	ISP	14.36	-0.12	-	-	-	-	-0.48	14.84	47.79	44.79
J0948.6+4041	1.25	FSRQ	LSP	13.51	0.50	0.81	12.71	41.39	44.04	-	-	-	-
J0957.6+5523	0.90	FSRQ	ISP	13.38	-0.15	-	-	-	-	-1.70	15.08	58.42	48.96
J0958.6+6534	0.37	BL Lac	LSP	14.15	-0.20	0.79	13.35	39.90	42.84	1.01	13.14	38.41	42.41
J1012.6+2439	1.80	FSRQ	LSP	13.86	0.83	-	-	-	-	-0.95	14.81	53.44	-
J1015.0+4925	0.21	BL Lac	HSP	15.53	-0.49	-	-	-	-	-0.80	16.33	50.84	-
J1033.2+4116	1.12	FSRQ	LSP	13.28	0.29	-	-	-	-	1.65	11.63	34.66	42.06
J1033.8+6051	1.40	FSRQ	LSP	13.66	0.37	-	-	-	-	-0.51	14.17	50.21	46.53
J1037.5+5711	-	BL Lac	ISP	-	-	-	-	-	-	-0.46	-	-	44.26
J1043.1+2407	0.56	FSRQ	LSP	14.72	-0.76	-	-	-	-	0.40	14.32	42.89	-
J1048.4+7144	1.15	FSRQ	LSP	13.69	0.45	-	-	-	-	0.34	13.35	44.35	-
J1058.5+0133	0.89	BL Lac	LSP	13.52	-0.20	1.09	12.43	38.98	43.44	-	-	-	-
J1058.6+5627	0.14	BL Lac	HSP	15.04	-0.44	-	-	-	-	-0.41	15.45	47.37	44.51
J1104.4+3812	0.03	BL Lac	HSP	16.43	-0.56	-	-	-	-	0.22	16.21	42.68	42.83
J1105.9+2814	0.84	FSRQ	LSP	13.91	0.59	-	-	-	-	0.65	13.25	41.58	-
J1112.4+3449	1.96	FSRQ	LSP	13.83	0.64	-	-	-	-	0.11	13.73	46.12	-
J1117.0+2014	0.14	BL Lac	HSP	16.35	-1.07	-	-	-	-	-0.59	16.94	48.83	-
J1124.1+2337	1.55	FSRQ	LSP	13.26	0.32	-	-	-	-	0.14	13.11	45.55	-
J1136.6+7009	0.05	BL Lac	HSP	15.87	-1.38	-	-	-	-	-0.30	16.17	45.97	44.08
J1150.3+2417	0.18	BL Lac	ISP	13.68	-0.45	-	-	-	-	-0.05	13.73	44.83	-
J1151.4+5858	-	BL Lac	ISP	-	-	-	-	-	-	-1.11	-	-	46.12
J1154.3+6023	1.12	FSRQ	LSP	13.71	1.58	-	-	-	-	0.90	12.81	40.65	42.72
J1159.5+2914	0.73	FSRQ	LSP	13.25	0.20	1.45	11.79	36.08	42.52	1.67	11.57	34.54	42.08

Table 1 continued.

3FGL name	z	opt.	SED	$\nu_{S,p}$	CD	δ_{var}	$\nu_{S,int}$	L_{bol}	$P_{j,int}$	δ_{eq}	$\nu_{S,int}$	L_{bol}	$P_{j,int}$
J1203.1+6029	0.07	BL Lac	ISP	14.65	-0.65	-	-	-	-	-0.26	14.91	45.26	43.97
J1209.4+4119	-	BL Lac	LSP	-	-	-	-	-	-	-0.24	-	-	43.62
J1217.8+3007	0.13	BL Lac	HSP	15.86	-0.99	-	-	-	-	0.17	15.70	43.88	43.58
J1220.2+7105	0.45	FSRQ	ISP	-	-	-	-	-	-	0.30	-	-	44.06
J1221.4+2814	0.10	BL Lac	ISP	14.20	-0.38	0.08	14.12	43.68	41.98	-0.14	14.34	45.19	42.42
J1224.6+4332	-	BL Lac	LSP	-	-	-	-	-	-	-0.20	-	-	46.14
J1224.9+2122	0.44	FSRQ	LSP	13.78	0.57	0.72	13.06	41.29	43.95	0.90	12.88	40.00	43.58
J1229.1+0202	0.16	FSRQ	LSP	13.34	0.52	1.23	12.11	37.75	43.04	-	-	-	-
J1230.3+2519	0.14	BL Lac	ISP	14.89	-0.64	-	-	-	-	-0.40	15.30	47.16	-
J1231.7+2847	0.24	BL Lac	ISP	15.19	-0.44	-	-	-	-	-0.58	15.77	48.86	46.37
J1243.1+3627	-	BL Lac	HSP	-	-	-	-	-	-	-0.76	-	-	45.23
J1248.2+5820	-	BL Lac	ISP	-	-	-	-	-	-	-0.11	-	-	44.73
J1253.2+5300	-	BL Lac	LSP	-	-	-	-	-	-	-0.24	-	-	44.64
J1256.1-0547	0.54	FSRQ	LSP	12.87	0.48	1.38	11.49	36.92	42.97	-	-	-	-
J1258.1+3233	0.81	FSRQ	LSP	13.42	0.20	-	-	-	-	-0.16	13.57	47.10	-
J1303.0+2435	0.99	BL Lac	LSP	14.03	0.30	-	-	-	-	0.48	13.55	42.55	-
J1308.7+3545	1.05	FSRQ	LSP	13.37	0.25	-	-	-	-	0.81	12.56	40.20	-
J1310.6+3222	1.00	FSRQ	LSP	13.53	-0.12	1.19	12.34	38.17	42.99	1.12	12.41	38.65	43.13
J1312.7+4828	0.64	AGN	LSP	13.17	0.74	-	-	-	-	-1.49	14.67	56.10	-
J1317.8+3429	1.05	FSRQ	LSP	13.53	0.36	-	-	-	-	-0.05	13.58	46.70	45.65
J1326.8+2211	1.40	FSRQ	LSP	13.43	0.47	1.33	12.10	37.56	42.46	1.39	12.04	37.13	42.34
J1331.8+4718	0.67	FSRQ	LSP	14.35	0.17	-	-	-	-	0.41	13.94	42.97	-
J1333.7+5057	1.36	FSRQ	ISP	14.13	1.07	-	-	-	-	-0.53	14.67	50.35	-
J1337.6-1257	0.54	FSRQ	LSP	13.37	-0.13	0.92	12.45	39.54	43.31	-	-	-	-
J1345.6+4453	2.53	FSRQ	LSP	13.55	1.04	-	-	-	-	0.63	12.92	43.15	-
J1350.8+3035	0.71	FSRQ	LSP	13.87	0.15	-	-	-	-	-0.18	14.06	47.08	-
J1357.6+7643	1.59	FSRQ	LSP	13.08	0.44	-	-	-	-	0.23	12.85	45.02	-
J1359.0+5544	1.01	FSRQ	ISP	13.53	1.35	-	-	-	-	0.10	13.43	45.89	-
J1416.0+1325	0.25	BCU I	LSP	13.55	-0.55	1.09	12.46	37.22	-	-	-	-	-
J1419.9+5425	0.15	BL Lac	LSP	13.98	-0.54	0.71	13.27	39.51	42.37	-	-	-	-
J1427.0+2347	-	BL Lac	HSP	-	-	-	-	-	-	-0.62	-	-	45.45
J1434.1+4203	1.24	FSRQ	LSP	-	-	-	-	-	-	-0.52	-	-	46.39
J1436.8+2322	1.54	FSRQ	LSP	13.49	-0.17	-	-	-	-	0.75	12.74	41.35	-
J1438.7+3710	2.40	FSRQ	LSP	12.95	0.86	-	-	-	-	0.66	12.29	42.43	-
J1443.9+2502	0.94	FSRQ	-	13.42	-0.19	-	-	-	-	0.36	13.06	43.20	-
J1454.5+5124	-	BL Lac	ISP	-	-	-	-	-	-	-0.93	-	-	47.13
J1504.4+1029	1.84	FSRQ	LSP	13.49	0.75	1.08	12.41	40.09	43.49	-0.15	13.64	48.70	45.95
J1506.1+3728	0.67	FSRQ	LSP	12.89	0.35	-	-	-	-	0.23	12.66	44.19	-
J1512.8-0906	0.36	FSRQ	LSP	13.58	0.96	1.22	12.36	37.89	42.48	-	-	-	-
J1516.9+1926	-	BL Lac	LSP	-	-	-	-	-	-	0.66	-	-	42.75
J1522.1+3144	1.49	FSRQ	LSP	13.42	1.58	-	-	-	-	0.35	13.07	45.09	-
J1539.5+2746	2.19	FSRQ	ISP	14.21	-0.31	-	-	-	-	0.29	13.93	44.65	-
J1540.8+1449	0.61	BL Lac	LSP	13.58	-0.81	0.63	12.94	41.32	43.99	-	-	-	-

Table 1 continued.

3FGL name	z	opt.	SED	$\nu_{S,p}$	CD	δ_{var}	$\nu_{S,int}$	L_{bol}	$P_{j,int}$	δ_{eq}	$\nu_{S,int}$	L_{bol}	$P_{j,int}$
J1542.9+6129	-	BL Lac	ISP	-	-	-	-	-	-	-0.32	-	-	43.83
J1553.5+1256	1.31	FSRQ	ISP	13.80	0.15	-	-	-	-	-0.62	14.42	51.10	46.75
J1604.6+5714	0.72	FSRQ	ISP	13.70	0.41	-	-	-	-	-0.69	14.39	50.93	-
J1607.0+1551	0.50	FSRQ	LSP	13.36	0.17	-	-	-	-	-0.20	13.56	46.84	45.21
J1608.6+1029	1.23	FSRQ	LSP	13.39	0.98	1.40	11.99	37.53	42.49	-0.08	13.47	47.90	45.46
J1613.8+3410	1.40	FSRQ	LSP	13.43	-0.80	1.14	12.29	38.95	43.03	-0.15	13.57	47.93	45.59
J1630.6+8232	0.02	RDG	LSP	14.29	-0.94	-	-	-	-	-0.55	14.84	46.59	-
J1635.2+3809	1.81	FSRQ	LSP	13.45	0.74	1.33	12.12	38.44	42.96	-	-	-	-
J1637.7+4715	0.74	FSRQ	LSP	13.06	0.32	-	-	-	-	0.18	12.88	44.75	45.06
J1637.9+5719	0.75	FSRQ	ISP	13.47	1.37	1.15	12.33	39.16	-	-	-	-	-
J1640.9+1142	0.08	BCU I	ISP	13.93	-0.60	-	-	-	-	-0.82	14.75	49.17	-
J1642.9+3950	0.59	FSRQ	LSP	13.60	-0.29	0.89	12.71	40.26	43.96	-	-	-	-
J1647.4+4950	0.05	BCU I	LSP	14.68	0.22	-	-	-	-	-0.39	15.07	46.25	-
J1656.9+6008	0.62	FSRQ	ISP	13.63	0.82	-	-	-	-	0.16	13.47	44.93	-
J1700.1+6829	0.30	FSRQ	LSP	13.36	0.87	-	-	-	-	0.16	13.20	44.15	44.04
J1709.6+4318	1.03	FSRQ	LSP	13.97	0.79	-	-	-	-	-0.36	14.33	48.88	-
J1719.2+1744	0.14	BL Lac	LSP	13.32	-0.27	-	-	-	-	0.52	12.79	40.32	42.51
J1722.7+1014	0.73	FSRQ	LSP	13.53	0.17	-	-	-	-	-0.41	13.94	48.78	-
J1727.1+4531	0.72	FSRQ	LSP	13.70	0.52	-	-	-	-	1.53	12.18	35.71	42.04
J1728.3+5013	0.06	BL Lac	HSP	15.98	-1.42	-	-	-	-	-0.86	16.84	49.94	45.00
J1728.5+0428	0.29	FSRQ	LSP	13.82	0.62	0.58	13.24	41.49	43.02	-	-	-	-
J1730.6+3711	0.20	BL Lac	ISP	14.68	-0.80	-	-	-	-	-1.42	16.10	54.18	-
J1733.0-1305	0.90	FSRQ	LSP	12.44	0.36	1.03	11.41	39.40	43.66	-	-	-	-
J1734.3+3858	0.98	FSRQ	LSP	13.27	0.31	-	-	-	-	0.39	12.88	43.56	-
J1740.3+5211	1.38	FSRQ	LSP	13.91	0.32	1.42	12.48	36.98	42.52	-	-	-	-
J1742.2+5947	-	BL Lac	ISP	-	-	-	-	-	-	-0.50	-	-	44.38
J1743.9+1934	0.08	BL Lac	HSP	15.23	-1.28	-	-	-	-	-0.65	15.87	48.64	45.11
J1744.3-0353	1.06	FSRQ	LSP	13.26	-0.57	1.29	11.97	37.13	-	-	-	-	-
J1748.6+7005	0.77	BL Lac	LSP	14.57	-0.49	-	-	-	-	-0.24	14.81	47.98	45.33
J1749.1+4322	-	BL Lac	LSP	-	-	-	-	-	-	0.11	-	-	43.81
J1751.5+0939	0.32	BL Lac	LSP	13.85	0.03	1.08	12.77	37.67	42.70	-	-	-	-
J1800.5+7827	0.68	BL Lac	LSP	13.76	-0.23	1.09	12.67	38.67	42.71	0.41	13.35	43.42	44.06
J1806.7+6949	0.05	BL Lac	ISP	14.20	-0.66	0.04	14.16	43.52	43.87	-0.05	14.25	44.16	44.05
J1813.6+3143	0.12	BL Lac	ISP	14.81	-0.75	-	-	-	-	-0.58	15.39	48.12	44.78
J1824.2+5649	0.66	BL Lac	LSP	13.73	0.23	0.81	12.92	40.66	43.79	0.56	13.17	42.37	44.28
J1829.6+4844	0.69	SSRQ	LSP	13.32	-0.89	0.76	12.56	41.36	-	-	-	-	-
J1848.4+3216	0.80	FSRQ	LSP	13.28	0.77	-	-	-	-	-0.15	13.43	47.31	-
J1849.2+6705	0.66	FSRQ	LSP	13.84	0.25	-	-	-	-	0.89	12.95	39.76	43.62
J1852.4+4856	1.25	FSRQ	LSP	13.53	0.58	-	-	-	-	1.17	12.36	38.17	-
J2000.0+6509	0.05	BL Lac	HSP	16.19	-0.84	-	-	-	-	-0.34	16.53	46.35	-
J2001.8+7041	0.25	BL Lac	HSP	13.52	-0.18	-	-	-	-	-0.95	14.47	50.83	-
J2005.2+7752	0.34	BL Lac	LSP	14.07	-0.60	1.12	12.94	37.51	42.08	0.29	13.78	43.36	43.75
J2022.5+7612	0.59	BL Lac	ISP	14.51	-0.28	-	-	-	-	0.38	14.14	43.24	-
J2031.8+1223	1.22	BL Lac	LSP	14.04	-0.20	-	-	-	-	0.98	13.06	39.85	-
J2035.3+1055	0.60	FSRQ	ISP	13.90	0.22	-	-	-	-	0.43	13.47	43.13	44.01

Table 1 continued.

3FGL name	z	opt.	SED	$\nu_{S,p}$	CD	δ_{var}	$\nu_{S,int}$	L_{bol}	$P_{j,int}$	δ_{eq}	$\nu_{S,int}$	L_{bol}	$P_{j,int}$
J2115.4+2933	1.51	FSRQ	LSP	13.33	0.25	-	-	-	-	-0.84	14.17	52.54	-
J2116.1+3339	1.60	BL Lac	HSP	15.35	-0.17	-	-	-	-	-1.05	16.40	54.14	-
J2121.0+1901	2.18	FSRQ	ISP	13.33	0.11	-	-	-	-	-0.35	13.68	49.32	-
J2123.6+0533	1.94	FSRQ	LSP	13.98	-0.92	1.18	12.79	38.55	-	-	-	-	-
J2143.5+1744	0.21	FSRQ	ISP	14.23	0.78	-	-	-	-	0.48	13.75	42.18	43.41
J2152.4+1735	0.87	BL Lac	LSP	13.83	-1.27	-	-	-	-	-0.52	14.35	49.57	-
J2202.7+4217	0.07	BL Lac	LSP	14.10	-0.36	0.86	13.24	38.59	41.72	-	-	-	-
J2203.4+1725	1.08	FSRQ	LSP	14.05	0.18	-	-	-	-	0.12	13.93	45.75	45.26
J2203.7+3143	0.29	FSRQ	LSP	14.52	2.25	0.83	13.70	42.23	-	-	-	-	-
J2212.0+2355	1.13	FSRQ	LSP	13.31	-0.10	-	-	-	-	0.41	12.89	43.16	-
J2217.0+2421	0.50	BL Lac	LSP	14.28	-0.68	-	-	-	-	0.82	13.46	39.83	43.14
J2225.8-0454	1.40	FSRQ	LSP	13.24	-0.44	1.20	12.04	38.70	43.88	-	-	-	-
J2229.7-0833	1.56	FSRQ	LSP	13.89	1.00	1.20	12.69	39.26	42.77	-	-	-	-
J2232.5+1143	1.04	FSRQ	LSP	13.42	0.41	1.19	12.23	38.99	43.33	-	-	-	-
J2236.3+2829	0.79	BL Lac	LSP	14.08	-0.13	0.78	13.30	40.91	-	0.72	13.36	41.32	-
J2250.1+3825	0.12	BL Lac	-	15.54	-0.90	-	-	-	-	-0.97	16.51	50.96	-
J2251.9+4031	0.23	BL Lac	ISP	14.25	0.03	-	-	-	-	-0.74	14.99	49.54	-
J2254.0+1608	0.86	FSRQ	LSP	13.64	0.76	1.52	12.12	37.12	42.82	1.07	12.57	40.26	43.71
J2311.0+3425	1.82	FSRQ	LSP	13.72	0.47	-	-	-	-	0.06	13.66	46.84	45.66
J2321.9+2732	1.25	FSRQ	LSP	13.63	-0.58	-	-	-	-	-0.07	13.70	47.00	-
J2321.9+3204	1.49	FSRQ	LSP	13.59	0.36	-	-	-	-	0.67	12.92	41.76	-
J2322.5+3436	0.10	BL Lac	HSP	15.27	-0.27	-	-	-	-	-0.87	16.14	50.06	-

Notes: Column 1 is the source name in the third Fermi-LAT catalog (3FGL, Acero et al. 2015). Columns 2-4 give the redshift, optical type and the SED classification in the 3LAC. Column 5 and Column 6 are the k-corrected synchrotron peak frequency in unit of Hz, and Compton Dominance. Column 7 is the Doppler factor estimated from radio variability. Columns 8-10 are the Doppler-corrected intrinsic synchrotron peak frequency in unit of Hz, intrinsic luminosity in unit of erg s^{-1}, and intrinsic jet power in unit of erg s^{-1} calculated with δ_{var}. Column 11 is the Doppler factor derived from VLBI observations. Columns 12-14 are the Doppler-corrected intrinsic synchrotron peak frequency in unit of Hz, intrinsic luminosity in unit of erg s^{-1}, and intrinsic jet power in unit of erg s^{-1} calculated with δ_{eq}. All the values except redshift are in logarithmic space.